

# Ions and Water Dancing through Atom-Scale Holes: A Perspective toward “Size Zero”

Jothi Priyanka Thiruraman, Paul Masih Das, and Marija Drndić\*



Cite This: <https://dx.doi.org/10.1021/acsnano.0c01625>



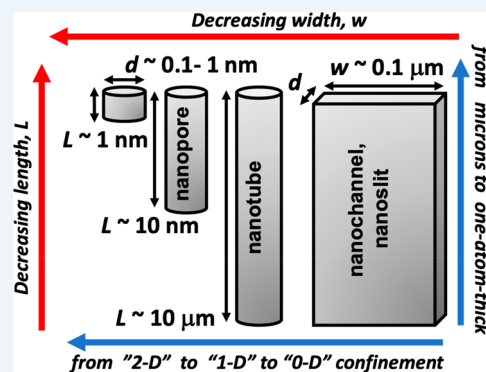
Read Online

ACCESS |

Metrics & More

Article Recommendations

**ABSTRACT:** We provide an overview of atom-scale apertures in solid-state membranes, from “pores” and “tubes” to “channels”, with characteristic sizes comparable to the sizes of ions and water molecules. In this regime of  $\sim 1$  nm diameter pores, water molecules and ions are strongly geometrically confined: the size of water molecules ( $\sim 0.3$  nm) and the size of “hydrated” ions in water ( $\sim 0.7$ – $1$  nm) are similar to the pore diameters, physically limiting the ion flow through the hole. The pore sizes are comparable to the classical Debye screening length governing the spatial range of electrostatic interaction,  $\sim 0.3$  to  $1$  nm for  $1$  to  $0.1$  M KCl. In such small structures, charges can be unscreened, leading to new effects. We discuss experiments on  $\sim 1$  nm diameter nanopores, with a focus on carbon nanotube pores and ion transport studies. Finally, we present an outlook for artificial “size zero” pores in the regime of small diameters and small thicknesses. Beyond mimicking protein channels in nature, solid-state pores may offer additional possibilities where sensing and control are performed at the pore, such as in electrically and optically addressable solid-state materials.



*For there seems to be no limit to the number of competing constructions, which, at least in principle, could claim to give a coherent and simple account of the available phenomena. This is due to the fact that theories are the result of human ingenuity.*

“Einstein, Science and Philosophy” by Friedel Weinert<sup>1</sup> With the advances of nanofabrication techniques and the growth and synthesis of new low-dimensional materials, such as nanotubes and graphene, it is possible to probe the fundamental principles of ion and molecule transport down to the single-atom scale. Many different artificial structures have been realized and tested such as low-dimensional nanopores and “nanoporous” membranes (see Danda *et al.*<sup>2</sup> for a recent review). In this interesting size regime (about  $1$  nm and below), single ions and molecules are only a few times smaller or even comparable to the characteristic size of the apertures through which they translocate. As a result, their interactions with the atoms of the structures can be significant and govern the types of phenomena observed. The geometrically restricted flow of ions and water can give rise to new phenomena where atomistic details become important and that can differ from the leading phenomena at larger scales. The single-atom and sub-nanometer scales are also typically regimes where, for many materials, simple calculations such as Ohm’s law for ion current *versus* pore size, which are otherwise typically

applicable for larger pores, fail. Macroscopic quantities such as bulk ion mobilities or bulk ion concentrations become inadequate and have to be modified within the pores to explain features of the measured ion conductance and its scaling with experimental parameters, such as ion concentration and net charges of the pore “walls” (edge atoms), which depend on the pH value.

In this Perspective, rather than providing a comprehensive review of important contributions, we instead discuss selected experimental progress on small-diameter apertures for fluid transport with a focus on carbon nanotube (CNT) pores, as featured in the November 2019 issue of *ACS Nano*,<sup>3</sup> and the related ion transport studies and provide our subjective outlook. We also focus on the experimental details and results while omitting discussions of theoretical modeling approaches. Small-diameter artificial pores mimic ion transport channels and pumps found in nature while offering new designs and opportunities, such as by using electrically conducting and optically responsive two-dimensional (2D) membranes.

**Sizes of Water Molecules and Ions and Comparably Small Apertures:  $\sim 0.1\text{--}1\text{ nm}$ .** In addition to the physical size of water molecules and common ions in solution, estimated to be  $\sim 0.3$  to  $\sim 1\text{ nm}$ ,<sup>4–7</sup> another relevant size scale to consider and to compare to characteristic nanostructure sizes is the Debye screening length,  $\lambda_D$ , which is a good estimate of how far the electrostatic effects of unscreened charges will persist (*i.e.*, the distance at which the electrostatic potential drops by a factor of  $1/e$ ). This characteristic length scale, obtained from Poisson's equation, governs the exponential decay of the electric potential away from the charges and describes the screening of a charge's electrostatic potential due to the net effect of the interactions it undergoes with the other mobile charges (electrons and ions) in the system. For concentrated ion solutions, such as 1 M KCl, this length is calculated to be  $\lambda_D \approx 0.3\text{ nm}$ , the size of one water molecule. It increases to  $\lambda_D \approx 1\text{ nm}$  for 0.1 M KCl, equivalent to about four water molecule diameters, and to  $\lambda_D \approx 10\text{ nm}$  for 1 mM KCl.<sup>2–4</sup> Therefore, as the size of the channels and nanostructures becomes smaller, it is more difficult for charges to be screened within that space, even for relatively high ion concentrations, and Coulomb interactions become important. An “ionic Coulomb blockade” was first suggested analytically and by means of molecular dynamics simulations<sup>8</sup> and recently reported for sub-1 nm diameter 2D monolayer MoS<sub>2</sub> nanopores.<sup>6</sup>

Another conceptually simple, classical length scale directly related to the Debye length, arising in phenomena in electrolytes, polyelectrolytes, and colloidal dispersions, is the Bjerrum length,  $\lambda_B$ , the separation at which the electrostatic interaction energy between two elementary charges is comparable in magnitude to the thermal energy:<sup>9</sup>

$$\lambda_B = \frac{e^2}{4\pi\epsilon_0\epsilon_r k_B T} \quad (1)$$

where  $k_B \approx 1.38 \times 10^{-23}\text{ m}^2\text{ kg s}^{-2}\text{ K}^{-1}$  is the Boltzmann constant,  $e = 1.6 \times 10^{-19}\text{ C}$  is the elementary charge,  $\epsilon_r$  is the relative dielectric constant,  $\epsilon_0$  is the vacuum permittivity, and  $T$  is temperature. For water at room temperature,  $\epsilon_r = 80$  so that  $\lambda_B \approx 0.7\text{ nm}$ . Roughly, we may assume that at separations smaller than  $\lambda_B$ , the Coulomb interaction between unit charges in water dominates compared to the thermal energy. The Debye length in electrolyte solution is  $\lambda_D \sim 1/\sqrt{\lambda_B I}$ , where  $I$  is the ionic strength, frequently expressed in molar (M).

Given the values of these characteristic length scales,  $\sim 0.1\text{--}1\text{ nm}$ , it is not surprising that some interpretations using equations underlined by assumptions valid only for large-scale ion flow channels may start to break down dielectrically for atom-scale apertures. Old terminology, concepts, and theoretical tools may not be applicable for these new atomic-transport problems. “All-atom” viewpoints, such as those put forth by

As described in the November 2019 issue of *ACS Nano*, Yao *et al.* probed ion and water transport through short, small-diameter carbon nanotubes with 1.5 nm diameters that were vertically embedded in lipid bilayer membranes.

molecular dynamics simulations, which analyze the more realistic movement of atoms and molecules and rely on appropriate potential functions, can be expected to have more

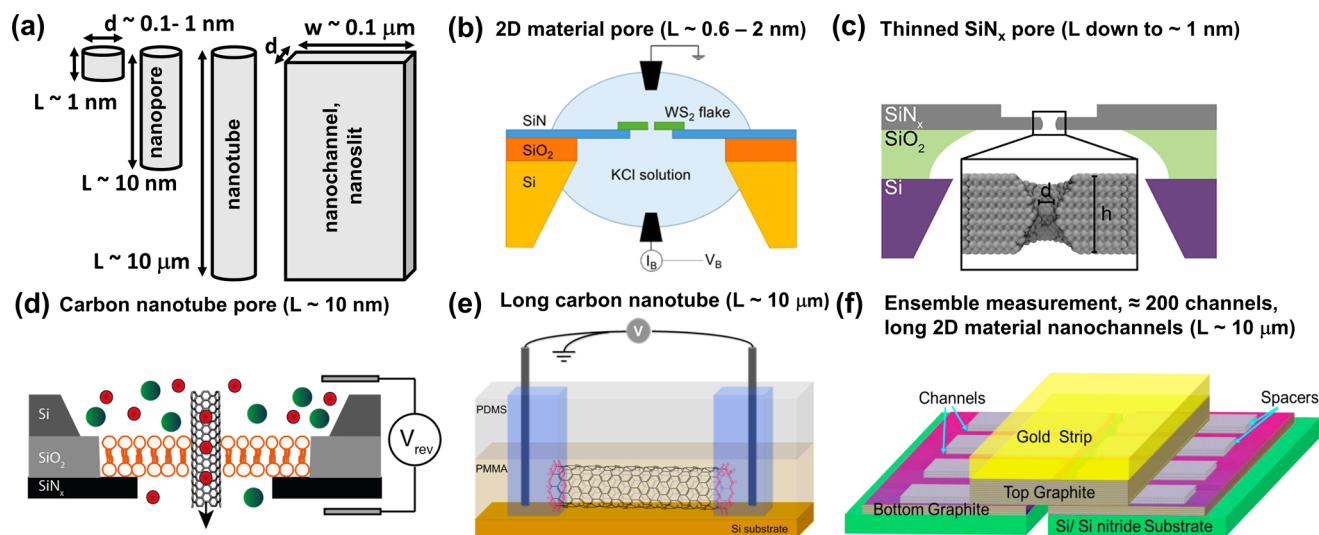


**Figure 1.** Overview of the relevant order of magnitude sizes of fluidic transport channels and selected examples of recently measured structures. Diameters,  $d$ , as small as the sizes of single-atom vacancies, on the order of 0.1 nm, can be achieved. (a) Channel length,  $L$ , can be tuned from  $\sim 0.1\text{ nm}$  to  $10\text{ }\mu\text{m}$ , corresponding to “pores” vs “tubes” and “channels”, as the dominant terminologies used in recent literature to describe such structures. Note that calculated sizes of water molecules are  $\sim 0.3\text{ nm}$  and of hydrated ions are  $0.7\text{--}1\text{ nm}$ .<sup>4,7</sup> (b–f) Examples of recent experiments and device configurations, shown in the order of increasing channel length, from  $L \sim 1\text{ nm}$  for “nanopores” as in two-dimensional (2D) pores made of graphene,<sup>25–27</sup> MoS<sub>2</sub>,<sup>28</sup> WS<sub>2</sub>,<sup>20</sup> BN,<sup>29,30</sup> MXenes,<sup>31</sup> sub-10 nm thick silicon nitride membranes,<sup>15–18,32</sup> and sub-7 nm thick HfO<sub>2</sub>,<sup>33</sup> to  $L \sim 10\text{ nm}$ , for “ultrashort” carbon nanotubes reported by Yao *et al.*<sup>3</sup> to long nanotubes,  $L \sim 10\text{ }\mu\text{m}$ ,<sup>12,13</sup> and similarly long, but 100 to 1000 times wider nanoslits made by stacking and patterning 2D materials.<sup>7</sup> Images adapted with permission from refs 20, 15, 3, 12, and 7. Copyrights 2017, 2013, 2019, and 2017 American Chemical Society and copyright 2017 American Association for the Advancement of Science, respectively.

predictive power than the older, mean-field and many-body approaches. Experimental outcomes now frequently depend on minute details and differences in atomic structures, and the corresponding models and theories should be able to reflect this standard.

Experimental approaches at the atomic scale can also suffer from significant errors and deficiencies resulting from the generally small numbers of samples from which conclusions are drawn due to challenges with working at this scale and the potential for sample contamination. In addition, it is reasonable to assume that there may be some preferential selection of devices and/or data that fit preconceived expectations and older theories. As we proceed in measuring, rationalizing, and theorizing atom-scale devices, it is important to determine related errors and to outline assumptions and limitations. It is with these upfront, cautionary notes that we proceed to discussing recent “atom-scale hole measurements”.

**Small-Size Apertures: Atom Vacancies, Porins, Tubes, Pores—“I’m a Small Hole with Many Names”.** As described in the November 2019 issue of *ACS Nano*, Yao *et al.* probed ion and water transport through short CNTs with 1.5 nm diameters that were vertically embedded in lipid bilayer membranes.<sup>3</sup> These carbon nanotubes can be considered as “pores” because they are relatively short ( $\sim 10$  nm long<sup>10</sup>), so that, effectively, when embedded vertically into a membrane, they act as single nanopores, mimicking protein pores and other artificial solid-state pores such as silicon nitride nanopores.<sup>11</sup>

The term “nanopore” or “pore” generally denotes a transport channel whose length is comparable to its diameter,  $d \approx L$  (Figure 1a). Conversely, the terms “nanotube” and “nanochannel” are typically used to denote a transport channel whose length is much larger than the channel diameter,  $d \ll L$ . For example, typical CNTs used to study ion transport are microns long,<sup>12</sup> with diameter-to-length ratio  $d/L \sim 1:10\,000$ , in contrast to the short carbon nanotubes used by Yao *et al.*,<sup>3</sup> with a ratio of  $d/L \approx 1:10$ . Researchers have studied the flow of water and ions through CNTs,<sup>10,12,13</sup> as well as through channels formed by patterning and stacking 2D material layers to form channels  $\sim 0.6$  nm thick, corresponding to the minimum separations between 2D layers in stacked graphene, boron nitride, and MoS<sub>2</sub>.<sup>7</sup>

Yao *et al.*<sup>3</sup> explain that, in CNT channels, which are on the same order of magnitude as the typical size of a solvated ion, the flow of ions and the flow of water are strongly coupled. The central finding of their paper is that this coupling manifests itself in the “unusual”  $2/3$  power-law scaling of conductance with ion concentration. The authors also propose these channels as a platform to create electro-osmotic pumps where low applied voltages could produce decent flows and operate at relatively high salinities. The nonlinear dependence of conductance on concentration also implied some negative surface charge on the inner CNT walls, the origin of which and other details have yet to be fully understood.<sup>3,10,13,14</sup>

Yao *et al.* demonstrated successful carbon nanotube devices that can be tuned to pass K<sup>+</sup> ions selectively.

In comparison to CNT channels, common protein pores have a similar diameter but are a bit shorter.  $\alpha$ -Hemolysin pores are about 5 nm thick with a diameter of  $\sim 1.4$  nm,

whereas MspA pores have a narrow constriction of about 0.6 nm thick with a diameter of  $\sim 1.2$  nm (see a comparison table in Venta *et al.*<sup>15</sup>). The short CNT pores (or porins, in analogy to biological systems) are also comparable in size to silicon nitride pores, although the thinnest silicon nitride pores can be even shorter, effectively as thin as  $\sim 1$  nm. Such thin membranes are typically formed by electron-beam thinning,<sup>16–18</sup> helium-beam thinning,<sup>19</sup> or, for example, more recently, laser illumination<sup>20–23</sup> in combination with electro-poration.<sup>24</sup> The minimum thickness of stable amorphous silicon membranes is predicted to be about 0.7 nm (about four silicon atoms thick membranes)<sup>16</sup> and approaching the 2D thickness limit. Like small-diameter CNTs, the 1–2 nm diameter range is also possible with silicon nitride pores. This diameter range is mostly desired for translocation experiments with single-stranded DNA molecules, whose diameter is about 1.1 nm, but smaller diameter pores below 1 nm can also be made, for example, in  $\sim 3$ – $5$  nm thick silicon nitride membranes.<sup>15,18</sup>

Figure 1 illustrates several different types of solid-state fluidic transport structures, including examples of 2D material pores,<sup>6,20,25–31,34–36</sup> silicon-<sup>15–18,32</sup> and hafnium-based<sup>33</sup> pores, CNTs,<sup>10,12,13</sup> and nanopatterned channels.<sup>7</sup> A concise and useful table comparing main characteristics of notable 2D pores was published by Mojtabavi *et al.* in their paper on MXene pores.<sup>31</sup> Other discussions can be found in a review by Danda *et al.*<sup>2</sup>

**Midsize Long Nanotubes and Nanochannels versus Shorter Nanopores.** For the thinnest and smallest diameter pores, one can consider using the term “quasi-zero-dimensional” (0D) to emphasize that, in contrast to long channels such as those defined by stacking 2D layers,<sup>7</sup> here the channel itself can be as short as a single atom. Graphene pores<sup>25,26</sup> and transition metal dichalcogenide (MoS<sub>2</sub> and WS<sub>2</sub>) pores<sup>20,28</sup> are  $\sim 0.6$  to  $\sim 1.6$  nm thick, respectively, and this “effective thickness” value was obtained from an analytical or a numerical fit (*e.g.*, molecular dynamics simulations for graphene nanopores<sup>37</sup>) of the ionic current measured through such thin pores. Experimentally, pores have to be cleaned and annealed to ensure a relatively clean 2D surface; otherwise, contamination can accumulate and pores can become thicker, giving large variations in reported ionic currents, surface charges, and selectivities. In addition, 2D pores<sup>6,21,38</sup> and the long channels made of 2D stacks can be soaked in ethanol<sup>7</sup> prior to filling them with salt solutions to aid in removing air bubbles and establishing ion and water flow. These structures are typically hydrophobic and difficult to wet.

In contrast to quasi-0D pores, only one dimension of  $\sim 10$   $\mu\text{m}$  long channels<sup>7</sup> is approaching the atomic scale—their thickness. To observe size effects in ion and water transport through confined volumes, it is sufficient to have at least one of the three spatial dimensions approaching the atomic scale, so that there is confinement in at least one dimension. For example, in very long and wide (0.1  $\mu\text{m}$ ) stacked graphene-based channels, when the channel height was minimized to  $\sim 0.6$  nm, the conductivity within the channel decreased with the increased “hydrated diameter” of ions used from 0.66 to 0.96 nm, due to the increasing spatial confinement of ions in channels of the fixed size.<sup>7</sup> The conductivity within the channel was calculated from measured conductance from 200 channels and was smaller than the bulk conductance values at corresponding molarities. Because of the long length of each channel ( $\sim 3$ – $7$   $\mu\text{m}$ ), the individual channel conductance was

Table 1. Comparison of Ionic Transport Properties in Selected Pore, Channel, and Tube Architectures<sup>a</sup>

Selected Ion Transport Experiments with Pores, Tubes, Channels (by Year of Publication)	Material	Pore Diameter (d)/Dimensions	Pore Fabrication Technique	Maximum Applied Voltage	Maximum Conductance/IV Linearity (in 1 M KCl)	Conductance (G) vs. Concentration (C) Dependence/Range Measured (in KCl)	Calculated Pore Surface Charge	Maximum Calculated K <sup>+</sup> /Cl <sup>-</sup> Selectivity Ratio	Type of Measurements	pH	Comments
Siria <i>et al.</i> , 2013 <sup>44</sup>	Boron nitride nanotubes (BNNTs)	Single tube; d = 30–80 nm, L = 1 μm	Nanomanipulation	100 mV	23 nS, linear	G saturates as C decreases below 0.1 M; 10 <sup>-4</sup> to 3 M	0.1 to 1 C/m <sup>2</sup>	N/A	Pressure-assisted ionic conductance	3.0 to 11	Osmotic energy conversion
O'Hern <i>et al.</i> , 2014 <sup>55</sup>	Monolayer graphene	Multiple pores; d = 0.2–0.6 nm, L = 0.6 nm	Ga ion irradiation and acid etching	N/A	N/A	N/A	N/A	1.3, Eq. (3)	Membrane potential	N/A	Cation-selective ionic transport
Rolling <i>et al.</i> , 2016 <sup>45</sup>	Monolayer graphene	Single pore; d = 2–20 nm, L = 0.6 nm	Breakdown, 5–7 V applied to make pore	150 mV	1 μS, linear	Power law dependence between G and C; 10 <sup>-2</sup> to 3 M	-0.6 to 0 C/m <sup>2</sup>	>100, Eq. (3)	Ionic conductance	2.0 to 8.0	Selectivity in pores up to d = 20 nm
Feng <i>et al.</i> , 2016 <sup>56</sup>	Monolayer MoS <sub>2</sub>	Single pore; d = 2–25 nm, L = 0.7 nm	Transmission electron microscopy (TEM) drilling or breakdown, 0.8 V applied to make pore	400 mV	500 nS, linear	G saturates as C decreases below 10 <sup>-3</sup> M; 10 <sup>-5</sup> to 1 M	-90 to -20 mC/m <sup>2</sup>	N/A	Ionic conductance	2.0 to 11	Nanopower generation
Tunuguntla <i>et al.</i> , 2017 <sup>16</sup>	Narrow carbon nanotube porins (nCNTPs)	Single and multiple tubes; d = 0.8 nm, L = 10 nm	Self-insertion into lipid bilayers	200 mV	180 pS, linear	Power law dependence (~C <sup>1/2</sup> ) between G and C; 4 × 10 <sup>-3</sup> to 3 M	N/A	184, Eq. (2)	Ionic conductance	3.0, 7.5, 7.8	nCNTPs are strongly cation selective
Esfandiari <i>et al.</i> , 2017 <sup>7</sup>	Graphene, MoS <sub>2</sub> , and hBN	Single and multiple channels; d = 0.6 nm, w = 0.13 μm, L = 3–7 μm	Electron beam lithography and dry etching	200 mV	30 nS, nonlinear (0.5 M)	G saturates as C decreases below 10 <sup>-4</sup> M; 10 <sup>-2</sup> to 1 M	20 to 300 μC/m <sup>2</sup>	~3, mobility ratio	Ionic conductance	2.0 to 10	Channels are selective to small cations (i.e., K <sup>+</sup> , Li <sup>+</sup> , Na <sup>+</sup> )
Amiri <i>et al.</i> , 2017 <sup>12</sup>	Single-wall carbon nanotubes (SWCNTs)	Single tube; d = 1.5 nm, L = 20 μm	Electron beam lithography and dry etching	400 mV	100 nS, N/A	Power law dependence (~C <sup>1/2</sup> ) between G and C; 10 <sup>-5</sup> to 1 M	N/A	121, permeability ratio	Ionic conductance through PMMA resist	2.0 to 8.0	Negative surface charges localized at nanotube entrance
Thiruraman <i>et al.</i> , 2018 <sup>58</sup>	Monolayer MoS <sub>2</sub>	Multiple pores; d = 0.2–0.8 nm, L = 0.7 nm	Ga ion irradiation	800 mV	40 nS, nonlinear	N/A	N/A	N/A	Ionic conductance	8.7	Tunable sub-nm defect production in monolayer MoS <sub>2</sub>
Chien <i>et al.</i> , 2019 <sup>18</sup>	SiN <sub>x</sub> /Si	Single pore; d = 0.9–2.4 nm, L = 3–8 nm	TEM thinning and drilling	900 mV	15 nS, N/A	N/A	~20 mC/m <sup>2</sup>	N/A	Ionic conductance	8.0	DNA translocations at 10 MHz bandwidth
Yao <i>et al.</i> , 2019 <sup>3</sup>	Wider carbon nanotube porins (wCNTPs)	Single tube; d = 1.5 nm, L = 10 nm	Self-insertion into lipid bilayers	100 mV	800 pS, linear	Power law dependence (~C <sup>2/3</sup> ) between G and C; 4 × 10 <sup>-3</sup> to 3 M	-75 to -20 mC/m <sup>2</sup>	~10, Eq. (2)	Ionic conductance	3.0, 7.5	Ionic transport dominated by strong electroosmotic coupling

<sup>a</sup>List of selected reports from the literature on low-dimensional porous systems. The dimensions, composition, and method of fabrication for various pores are given in addition to ionic transport characteristics such as ionic conductance,  $G$ ; scaling with ion concentration,  $C$ ; surface charge; and ion selectivity ratio. Unless noted, we report values for 1 M KCl solution.

smaller than the current measurement threshold for concentrations below 0.01 M, and the authors opted to instead perform measurements on ensembles of channels in order to obtain data at lower concentration,  $\sim 10^{-4}$  M KCl.<sup>7</sup>

**Scaling of Ion Current with Applied Voltage and with Bulk Ion Concentration: The Regime of Small Diameters.** Table 1 summarizes the details of recent measurements of small-diameter systems including their pore sizes, applied voltage, measured conductance, and other measured and calculated parameters including ion selectivity. Results are listed in the order of the year published.

In these systems, the typical first measurement involves immersing the sample in solution and, if the relatively delicate structure does not break during handling, determining the dependence of the ion current,  $I$ , on the externally applied voltage,  $V$ . Voltage is limited to  $\sim 100$  mV and maximum  $\approx 1$  V for slightly larger structures; for larger voltages, the sample breaks down, dielectrically or otherwise, as the electric field reaches  $\sim 0.1$ – $1$  V/nm across the membrane, which is sufficient to ionize atoms of the membrane material. The nonzero magnitude of the current in the pA to nA range and the lack of hysteresis are good indications that ion transport is occurring. When the  $I$ – $V$  relationship is linear, one can both define the slope, which is the ion conductance,  $G$ , and also consider its dependence on the ion concentration. In the case of nonlinear  $I$ – $V$  curves,  $G$  is not well-defined and the slope of the current at zero voltage can be used to estimate a

conductance value. Another directly measured quantity is the bulk concentration,  $C$ , or the ion concentration used in the experiment; the ion concentrations and mobilities within the constricted regions are different than bulk conductivities for these restricted ion flows. Pore conductivity and ion mobilities are sometimes calculated from the measured conductance and some assumed transport model,  $G$  versus size, either analytically or from numerical simulations (see example of 2D channels<sup>7</sup>), to show that they are smaller than bulk values.

From Table 1, maximum conductance,  $G$ , for 1 M KCl, ranges across 4 orders of magnitude from  $G \approx 180$  pS to  $G \approx 1$  μS for characteristic minimum aperture sizes of  $\sim 0.2$  to  $\sim 80$  nm. It is reassuring that these collective results on different structures seem generally consistent with the expected trends that short pores usually exhibit  $G$  larger than that for long tubes of the same diameter, and that larger-diameter pores show  $G$  larger than that of small-diameter pores of the same  $L$ . For example, we can directly compare the conductance of 20 μm long ( $G_{\text{longCNT}} \approx 100$  nS)<sup>12</sup> versus 13 nm long CNTs ( $G_{\text{shortCNT}} \approx 800$  pS)<sup>3</sup> of the same diameter,  $d = 1.5$  nm. From a simple length scaling between the two, the short CNTs should show a conductance 1500 times smaller, that is,  $G_{\text{shortCNT}}$  (from scaling)  $\approx 70$  pS, which is within 1 order of magnitude from what was measured.<sup>3</sup>

**Ionic Selectivity of Carbon Nanotubes, Nanopores, and Channels.** Many recent experiments have focused on the concept of “ion selectivity”, a calculated quantity discussed

below that is viewed as a particularly important aspect of these systems. Solid-state nanopores, nanotubes, and nanochannels have increasingly been reported to be “K<sup>+</sup> ion selective” (or “cation selective”) meaning that they only or preferentially allow K<sup>+</sup> ions to pass through while impeding others. Researchers have carried out experiments on a variety of pores, tubes, and channels made out of a wide range of low-dimensional solid-state materials (see Table 1) in conventional KCl solution. Carbon nanotubes are excellent candidates for such experiments because the surface can be functionalized using appropriate pH for ion-selective transport. Yao *et al.* demonstrated successful CNT devices that can be tuned to pass K<sup>+</sup> ions selectively.<sup>3</sup> They hypothesized that due to the presence of carboxyl groups (COO<sup>-</sup>) at the pore edge, neutral or higher pH helps keep the pore charged and, thus, the pore attracts more K<sup>+</sup> ions. In contrast, in acidic pH, the negative charge on the pore’s rim created by COO<sup>-</sup> groups is neutralized by COO<sup>-</sup> being protonated to form COOH). The authors also analyzed noise properties and power-law dependence of the noise on frequency and found a 1/*f* dependence similar to that of other solid-state pores such as silicon nitride<sup>39</sup> and graphene pores.<sup>25</sup> They report that noise decreases with increasing ion concentrations for pH 7.5, for which the pore is charged, suggesting that more screening of the pore charge means lower noise.

The concept of ion selectivity is analogous to and borrowed from the field of ion channels and ion pumps found in nature (e.g., protein molecules that span across the cell membrane),<sup>40,41</sup> which already existed at these small scales before the solid-state structures were possible. Ion channels can enable the passage of certain ions while blocking others, thus playing important roles in controlling neuronal excitability. Specifically, some biological channels allow the flow of K<sup>+</sup> ions effectively but do not allow Na<sup>+</sup> ions to cross the membrane. Ion passage through the “K<sup>+</sup> channel selectivity filter” is believed to proceed as 2–3 K<sup>+</sup> ions interspersed by water molecules move in a single file, whereas permeation through the wider and less selective Na<sup>+</sup> channels proceeds similarly, although the ions may not be dehydrated.<sup>40</sup> Simple structural concepts like these and schematics of how ions pass through these channels are often invoked in biology to rationalize the mechanism of ion selectivity.

From ionic transport measurements, Yao *et al.* inferred strong electro-osmotic coupling between the ions and water molecules as they flow, based on the dependence of the conductance on concentration,  $G \sim C^{2/3}$  (in contrast, for example, to a linear scaling for simple ionic resistors).<sup>3</sup> This scaling exponent was obtained by fitting  $G$  versus  $C$  across approximately 2 orders of magnitude in  $G$  and in  $C$ . Conductance measurements spanning a greater range in molarity would increase the confidence level in the reported value of the fitted power-law exponent. Measuring ensembles of CNT pores would maximize the conductance at lower concentrations to increase its measurability, as was done for ~200 2D nanochannels.<sup>7</sup> In many solid-state nanopores and channels, conductance is limited by the surface charge of the pore and saturates at low concentrations,<sup>42,43</sup> and reported surface charge density is dependent on pH and varies by several orders of magnitude, both positively and negatively, from ~μC/m<sup>2</sup> in 2D stacked channels,<sup>7</sup> to ~mC/m<sup>2</sup> in silicon nitride,<sup>43</sup> MoS<sub>2</sub> pores,<sup>36</sup> and short CNTs,<sup>3</sup> to C/m<sup>2</sup> in boron nitride nanotubes<sup>44</sup> and graphene nanopores<sup>45</sup> (see Table 1). This is by no means a careful overview of all the values and

experimental details reported for such systems, but it is already sufficient to note the large variation of charge densities, across 6 orders of magnitude. We also note that, in many cases, the surface charge density is inferred from a fit of  $G$  versus  $C$ , and there are significant errors associated with these fits.

To evaluate ion selectivity quantitatively, a salt concentration gradient is set up, at zero applied voltage, and both K<sup>+</sup> and Cl<sup>-</sup> ions diffuse from high to low concentration. When the rate of diffusion of the ion (K<sup>+</sup>) is higher than that of the counterion (in this case Cl<sup>-</sup>), a net current (also known as short-circuit current because the external voltage is zero) is produced across the pore. Diffusion potential or reverse potential (also called open-circuit voltage) is referred to as the value of external voltage that can be applied to set the net current to zero. This selectivity (i.e., larger diffusion rate of the ion compared to its counterion) is governed by the pore size and surface chemistry. The pH of the solution plays an influential role together with the intrinsic surface charge of the material. Depending on the salt concentration, a cloud of counterions is created in response to the total surface charge of the pore material, known as the electric double layer (EDL). The spatial extent of this layer is defined by the Debye length  $\lambda_D$ . In the case of pore dimensions approaching this Debye length, the EDL can overlap, causing an excess concentration of counterions in the channel. Further, these excess counterions can then dominate ionic transport through the channel.<sup>46–48</sup>

To quantify ionic selectivity, the diffusion potential (equal to the external voltage applied to set the measured current to zero) is given as

$$V_{\text{rev}} = (2t_+ - 1) \frac{RT}{F} \ln \frac{c_{\text{top}}}{c_{\text{bottom}}} \quad (2)$$

in the form that Yao *et al.*<sup>3</sup> suggest, where  $R$  is the universal gas constant (8.314 J mol<sup>-1</sup> K<sup>-1</sup>),  $T$  is temperature,  $F$  is Faraday’s constant (96.485 C mol<sup>-1</sup>), and  $c_{\text{top}}$  and  $c_{\text{bottom}}$  are the electrolyte concentration on either side of the chamber. In the work by Yao *et al.*,  $c_{\text{bottom}}$  was fixed at 10 mM and  $c_{\text{top}}$  was increased from 10 to 600 mM (Figure 2a).<sup>3</sup> The authors define “ $t_+$ ” as the “transference number” for the cation, that is, the fraction of electrical current carried by the cation under the influence of applied voltage. The transference number can serve as an index of the ion selectivity,  $t_+ = 1$  or 0 for complete cation or anion selectivity, respectively. Hence,  $t_+ = 0.5$  corresponds to a non-ion-selective channel ( $V_{\text{rev}} = 0$  for  $t_+ = 0.5$  in eq 1).

The form of eq 2 can be contrasted with another form for the reverse potential that was used by Rollings *et al.*<sup>45</sup> for graphene nanopores:

$$V_{\text{rev}} = \frac{k_B T}{e} n \left( \frac{S_{\text{GHK}} c_{\text{high}} + c_{\text{low}}}{S_{\text{GHK}} c_{\text{low}} + c_{\text{high}}} \right) \quad (3)$$

where  $k_B \approx 1.38 \times 10^{-23}$  m<sup>2</sup> kg s<sup>-2</sup> K<sup>-1</sup> is the Boltzmann constant,  $e = 1.6 \times 10^{-19}$  C is the electron charge,  $S_{\text{GHK}}$  is the selectivity ratio (GHK stands for the Goldman–Hodgkin–Katz model), and  $c_{\text{high}}$  and  $c_{\text{low}}$  are the high and low concentrations, respectively, on the two sides of the membrane.

Slightly different terminology and different forms of these equations are used; for example, see studies of 2D graphite/MoS<sub>2</sub> nanochannels (Figure 2b) and 2D MoS<sub>2</sub> nanopores (Figure 2c).<sup>36</sup> Values of reported selectivity ratios,  $S$ , for

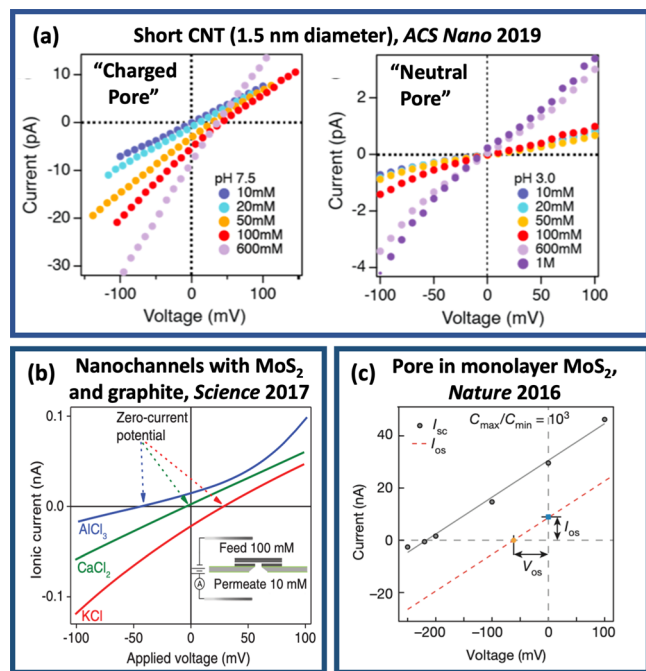


**Figure 2.** Current–voltage measurements for asymmetric ion concentrations on the two sides of a membrane, used to measure the “reverse potential” or “zero-current potential” across the pore. These measurements are performed to determine the extent to which current is carried by the positive and negative ions: (a) single, 1.5 nm diameter,  $\approx 13$  nm long carbon nanotube (CNT) with 10 mM to 600 mM KCl on one side and 10 mM on the other side of the membrane, for pH 7.5 (pore is charged) and pH 3 (pore is neutral), respectively;<sup>3</sup> (b)  $\approx 200$ , 0.6 nm thick ( $\sim 0.13$   $\mu\text{m}$  wide and 3–7  $\mu\text{m}$  long) parallel graphite/MoS<sub>2</sub> nanochannels in 100 mM/10 mM KCl, CaCl<sub>2</sub>, and AlCl<sub>3</sub> (this is an ensemble measurement rather than a single channel measurement);<sup>7</sup> and (c) single, 15 nm diameter two-dimensional MoS<sub>2</sub> nanopore in 1 M/1 mM KCl.<sup>36</sup> In (b), in the case of CaCl<sub>2</sub> and AlCl<sub>3</sub> solutions, the current at zero applied voltage is approximately zero and positive, respectively; positive current means that anions (Cl<sup>−</sup>) have a higher mobility than cations. Images adapted with permission from refs 3, 7, and 36. Copyrights 2019 American Chemical Society, 2017 American Association for the Advancement of Science, and 2016 Springer Nature, respectively.

related systems are listed in Table 1. Although the ways in which selectivity is measured and calculated and the structures and their fabrication methods differ across various studies, the one observation that appears consistent is that ionic selectivity occurs for neutral pH or higher (see Table 1).

**Short Carbon Nanotubes.** In the case of CNTs, Yao *et al.* observed a weak K<sup>+</sup> selectivity at pH of 7.5 (Figure 2a).<sup>3</sup> It is interesting to note that this concentration range corresponds to an EDL of 3 to 0.4 nm, similar to the pore CNT diameter, 1.5 nm. The region of K<sup>+</sup> is built up in response to the negatively charged CNT nanopore rim. In their work, the authors define “permselectivity”,  $P = \frac{t_+ - t_{+\text{bulk}}}{1 - t_{+\text{bulk}}}$ , where  $t_+$  and  $t_-$  are the transference numbers (the ratio of current derived from the K<sup>+</sup> ions to the total current produced) for positively and negatively charged ions and  $t_{+\text{bulk}} = 0.49$  for KCl solution. This investigation is similar and consistent with their previous CNT study,<sup>10</sup> in which they observe similar K<sup>+</sup> selectivity that they attributed to the negatively charged (COO<sup>−</sup>) rim of the pores at pH 7.5 or higher. They observed weak Cl<sup>−</sup> selectivity with

CNTs at pH 3 for 0.8 nm diameter tubes,<sup>10</sup> but wider, 1.5 nm diameter tubes were not ion selective at the same pH.<sup>3</sup> It is interesting to appreciate what a small difference in diameter of 0.7 nm can do in this size range.

**Two-Dimensional Nanopores.** Similar cation (K<sup>+</sup>) selectivity has been investigated for a range of nanopores (a few nanometer diameter to 20 nm diameter pores) in materials such as graphene<sup>45</sup> and MoS<sub>2</sub>.<sup>36</sup> In the case of few nanometer diameter ( $d = 2\text{--}25$  nm) 2D MoS<sub>2</sub> pores, Feng *et al.* calculated a decrease in ionic selectivity from 0.62 to 0.23 as the pore size increased from 2 to 25 nm.<sup>36</sup> Rollings *et al.* investigated graphene nanopores made using dielectric breakdown with diameters up to 20 nm and concluded that ionic selectivity  $S_{\text{GHK}} > 100$  (eq 2) was independent of pore diameter.<sup>45</sup> More recently, Caglar *et al.* studied ion selectivity in randomly defective graphene and hBN membranes deposited on glass capillaries and found that  $\sim 500$  anions per each cation get transported across the membrane in the case of a multivalent hafnium tetrachloride (HfCl<sub>4</sub>) salt solution.<sup>49</sup> These authors also used a variation of the Goldman–Hodgkin–Katz (GHK) equation and model to extract their quoted selectivity ratios. Their samples seem to contain random, irregularly shaped pores with a large size distribution with diameters up to  $\sim 30$  nm. One positive aspect of these samples is that they rely on random defects in material rather than a sophisticated pore fabrication method that may be timely and costly. However, in this case, it is then challenging to study systematically the fundamental aspects of selectivity as a function of pore properties if they are random.

Thiruraman *et al.* previously fabricated well-characterized ensembles of much smaller (sub-nanometer) pores in monolayer MoS<sub>2</sub> using Ga ion irradiation and observed a nonlinear current–voltage relationship through these pores for a range of irradiation doses corresponding to different pore size distributions.<sup>38</sup> They observed suppressed low-bias conductance compared to larger-diameter pores and extracted a simple scaling of conductance with effective pore diameter as  $G \approx 9 \text{ S/m} \times (d - 0.7 \text{ nm})$  in 1 M KCl, where  $d$  is the diameter in nanometers and 0.7 nm is the minimum pore diameter for ionic flow. Moreover, for such atom-scale pores, the concept of characteristic pore “diameter” or pore “size” could be further discussed and possibly redefined given that pore cross sections are not circular but rather have a well-defined atomic structure and edge terminations. There are a variety of 2D pore shapes and structural options to consider.<sup>38</sup> Liu *et al.* compared and contrasted the properties of few-nanometer-size triangular h-BN nanopores versus circular MoS<sub>2</sub> nanopores in DNA translocation experiments.<sup>50</sup> The pore resistance for the triangular pore had to be modified compared to circular pores. Similarly, from the atomic structure of angstrom-size MoS<sub>2</sub> pores, one can plot the distribution of “diameters” measured from the center of mass of the pore.<sup>38</sup>

For MoS<sub>2</sub> pores with diameters below  $\sim 2.0$  nm, the behaviors of the concentration and mobility of ions strongly deviate from bulk properties. Ion concentration, mobilities, and hydration are different than their bulk counterparts, as was already shown previously for graphene nanopores using molecular dynamics (MD) simulations by Suk *et al.*<sup>51</sup> Wilson *et al.* used MD to model 3.5 nm diameter graphene pores and observed that at  $\sim 500$  mV to 1 V applied across the membrane, water molecules will polarize and the electric field will compress the polarized molecules inside of the pore, thus creating outward pressure.<sup>52</sup> Atomic structures of single-

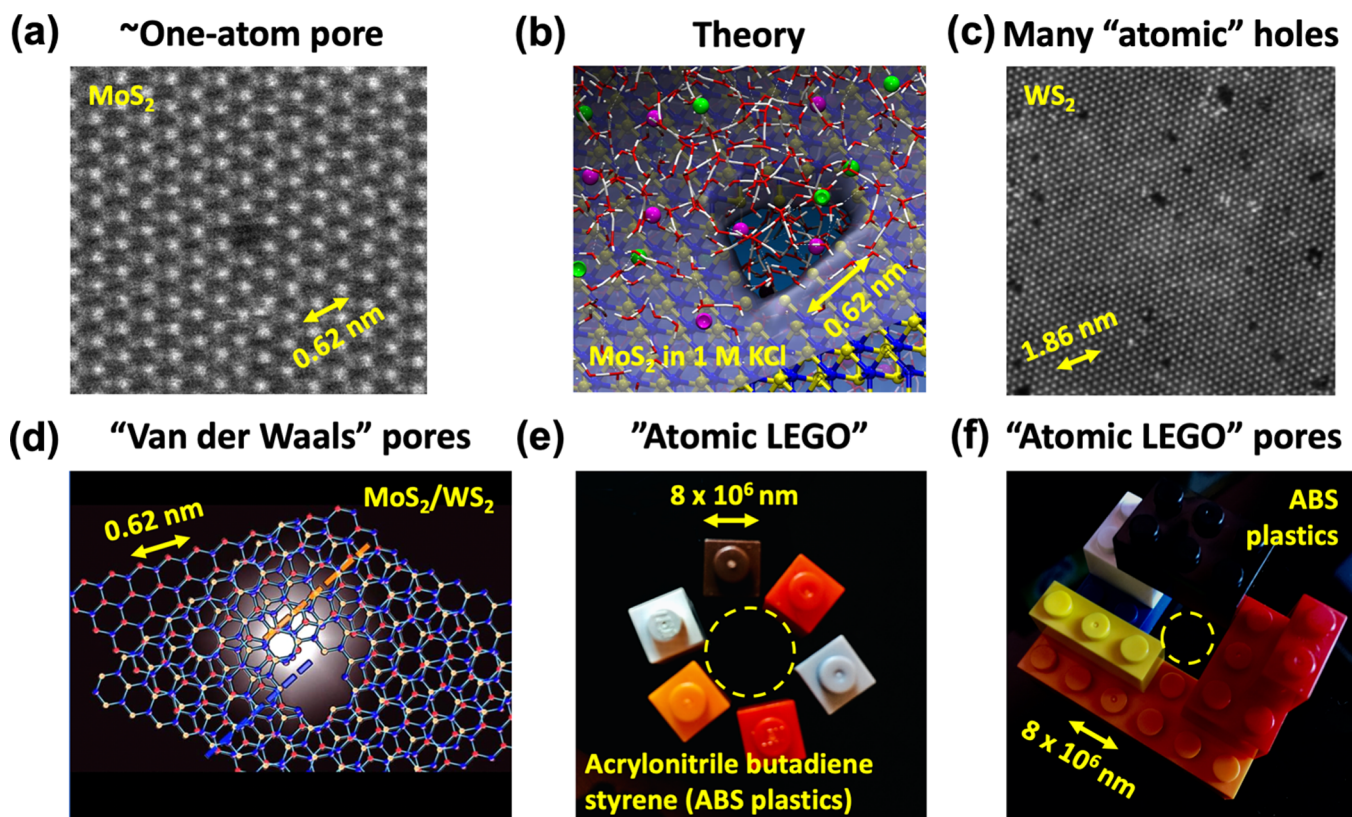


**Figure 3.** There are many opportunities for “size zero” two-dimensional (2D) and three-dimensional (3D) pores. (a) Aberration-corrected transmission electron microscopy (AC-TEM) image of an “approximately one-atom pore” made by electron beam drilling of the 2D MoS<sub>2</sub> membrane in the TEM. (b) Molecular dynamics model of water and K<sup>+</sup> and Cl<sup>-</sup> ion flow through sub-nanometer diameter 2D MoS<sub>2</sub> pores used for modeling ion-irradiated membranes with many atomic-scale holes, as in the TEM image shown in (c). (c) AC-TEM image of 2D WS<sub>2</sub> membrane after Ga ion irradiation using the Ga irradiation doses from previous works.<sup>38,60</sup> (d) Schematic of a pore drilled in two 2D material layers, monolayer MoS<sub>2</sub> on top of monolayer WS<sub>2</sub>.<sup>70</sup> (e,f) Inspired by Geim and Grigorieva,<sup>68</sup> this exquisite level of structural control is reminiscent of atomic-scale LEGO. Here, the pore edge is formed by adding 1 × 1 blocks. For ionic measurements, these edge atoms are particularly important. Three-dimensional, “size zero” atomic pores in 2D bilayers have been formed by stacking and patterning 2D materials and removing atoms from individual layers, also illustrated here by LEGO blocks. The removal of atoms can proceed selectively, one layer at a time, by selective beam irradiation.<sup>70</sup> Image credits: (a) Dr. William Parkin for making and imaging the 2D MoS<sub>2</sub> pore by electron irradiation in AC-TEM, (b) Prof. Adrien Nicolai for the molecular dynamics model,<sup>38</sup> (c) Paul Masih Das and Jothi Priyanka Thiruraman for making and imaging the ion-irradiated 2D WS<sub>2</sub> membrane in AC-TEM, (d) Milivoj Segan for making the illustration based on our TEM image, (e,f) Gabriela Buvac-Drndic for LEGO pores.

layer MoS<sub>2</sub> nanopores were also modeled by an equilibrium “all-atom” MD model (see also Figure 3b) in 1 M KCl to estimate the ratio between pore and KCl bulk conductivity,  $\sigma$ , showing a drop from  $\sigma_{\text{pore}}/\sigma_{\text{bulk}} \sim 80$  to 10% with the decrease in the effective pore diameter from  $\sim 2.5$  to  $\sim 0.7$  nm.<sup>53</sup> Non-equilibrium MD simulations assuming an applied external voltage were then used to develop an analytical expression for conductance, which is convenient for direct comparisons with experiments.<sup>54</sup>

In other work on graphene, O’Hern and colleagues showed a selectivity of 1.3 in graphene sub-nanometer diameter pores that were fabricated using ion beam irradiation of graphene to make holes and further processed in an acidic etchant to enlarge them.<sup>55,56</sup> The diameters of pores created in this process were shown to be  $< 1$  nm. There are also other, more robust, laminate and much thicker (few-microns-thick) membranes, such as graphene oxide (GO) membranes<sup>57</sup> and laminate MoS<sub>2</sub>,<sup>58</sup> some of which have been shown to be ion selective and are being commercialized for applications in the near future.

**Two-Dimensional Nanochannels.** Silica nanochannels have been studied for decades with regard to ionic transport

and power generation in the presence of a concentration gradient. Specifically, Kim *et al.* demonstrated power generation of  $\sim 8$  W/m<sup>2</sup> with an efficiency of  $\sim 30\%$ .<sup>47</sup> Although arrays of nanopores in 2D materials (MoS<sub>2</sub>) have been envisioned as possibly producing power densities in the range of MW/m<sup>2</sup> based on a simple scaling of results from single pores, this is yet to be realized.<sup>36</sup> Recently, Esfandiar *et al.* realized a variety of 2D channels fabricated using hBN, MoS<sub>2</sub>, and graphite.<sup>7</sup> In this work, they also measured the zero-current potential (here as “ $E_m$ ”) and observed that K<sup>+</sup> and Al<sup>3+</sup> diffuse through nanochannels faster and slower, respectively, compared to Cl<sup>-</sup> (Figure 2b). Further, they used the Henderson equation to calculate the ratio of ion mobilities. The authors concluded that, in the case of such 2D nanochannels, they detected a decrease in Cl<sup>-</sup> mobility ( $\sim 2 \times 10^{-8}$  m<sup>2</sup> V<sup>-1</sup> s<sup>-1</sup>) from K<sup>+</sup> ( $\sim 7 \times 10^{-8}$  m<sup>2</sup> V<sup>-1</sup> s<sup>-1</sup>) in the channel and speculated that it arises from polarization of water molecules around the ions. In analogy to ion transport, there is increasing work in gas transport through similar structures, but this is beyond the scope of our Perspective.

**Realization of “Size Zero” Apertures: From One-Dimensional Tubes to Zero-Dimensional Pores.** Fab-

rication of nanostructures and constricted geometries at the atomic scale, in general, can proceed either “bottom up” involving chemical synthesis or growth of structures “from the bottom” or “top down” involving patterning and etching methods to define the geometries “from the top”. This jargon is typically used to delineate the more chemistry-oriented *versus* physics-oriented approaches, respectively. Both approaches have been successful in producing nanometer and sub-nanometer scale apertures and channels for ion and water transport, with varying degrees of atomic-scale control, reproducibility, ease of fabrication, *etc.*

In the case of CNTs, as presented by Yao *et al.*, short CNTs were synthesized and cut by sonification from micron-long CNTs.<sup>3</sup> Rectangular channels with one dimension comparable to the atomic scales can be patterned by stacking 2D layers and then using lithography and etching to make channels, followed by capping the structure with another 2D layer.<sup>7</sup> In this fashion, the channel heights could be tuned in discrete increments of layer thickness, from monolayer-thick ( $\sim 0.6$  nm) to few-layer-thick channels.

The regime of quasi-zero thickness has also been achieved with suspended 2D membranes. Graphene, being planar and only one carbon atom thick, presents the ultimately thin nanopore.<sup>25,34</sup> For practical purposes, the effective thickness of graphene membranes in 1 M KCl solution is about 0.6 nm, obtained by fitting the ionic conductance *versus* pore diameter.<sup>26</sup> Such “2D” membranes can be made porous in a variety of ways, for example, using irradiation from various sources including electron<sup>59</sup> and ion irradiation, such as with Ga ion beams<sup>38,60</sup> and noble gas (He, Ne, Ar) ion beams<sup>61</sup> (for a recent overview of different nanopore fabrication methods, see Danda *et al.*<sup>2</sup>). Bombardment of membranes by energetic particles creates defects and vacancies, some of which have been considered beneficial for tailoring the material’s properties. For example, periodically patterned holes in graphene<sup>62</sup> and phosphorene<sup>63</sup> (also called “antidots”) leave behind a pattern of thin nanoconstrictions, whose widths, in turn, determine the new band gap of the resulting, leftover material. Wet chemical etching may be another promising route to make holes, such as demonstrated by using a combination of acids to etch 2D MoS<sub>2</sub> membranes, for example.<sup>64</sup>

There are more avenues to be explored toward facile and scalable fabrication approaches. Membranes with intentionally designed vacancies and holes could probably also be grown directly, and 2D sheets could be deposited on sharp pillars to induce strain<sup>65</sup> and potentially to make holes. For example, prepatterned or precorrugated surfaces could be used to grow 2D materials directly and possibly to pattern topological defects within 2D materials<sup>66</sup> and holes during the growth itself. Similarly, the curvature of the substrate can preferentially stabilize a specific number of 2D layers, such as in the recent work where trilayer graphene was grown by utilizing the curvature of the substrate.<sup>67</sup>

## OUTLOOK AND FUTURE DIRECTIONS

Understanding and control of ion and water flow through restricted volumes will expand current applications and enable new possibilities for applications, as well, including carbon nanotubes, nanochannels, and nanopores. Such apertures are reminiscent of biological ion channels, where similar levels of ionic currents are observed, in the pA range at  $\sim 100$  mV.<sup>40</sup> Membranes containing a large number of sub-nanometer pores may be important for the filtration of small molecules, for

selective flow of ions, and for applications including water desalination and energy harvesting. Yao *et al.* envision next-generation biomimetic membranes and pumps.<sup>3</sup> By controlling the ion concentration on both sides of the membrane, the pH value, the pore “wall” and membrane charges, and other physical and chemical properties of the pore and membrane materials, different transport regimes, could be realized.

**Understanding and control of ion and water flow through restricted volumes will expand current applications and enable new possibilities for applications as well, including carbon nanotubes, nanochannels, and nanopores.**

Making membranes and devices robust and scalable to larger areas and reproducing and verifying the observed phenomena across various laboratories will additionally propel the field forward. This undertaking is particularly important given that these structures have exposed surfaces that can easily be contaminated or changed during different experimental procedures. The atomic structure of holes (Figure 3a) can be now correlated, in principle, to their properties and performance in solution (Figure 3b), and it is possible that holes can be precisely, atomically engineered to achieve desired properties, such as to attract one type of ion while repelling another. As exemplified in the work by Yao *et al.*, theoretical modeling can be improved by considering atomistic details and new approaches of looking at these systems and can encompass a range of analytical and numerical approaches.<sup>3</sup> The advancement of large-scale computing and machine-learning approaches could aid in characterizing the various systems of defects and vacancies in materials and in preselecting or suggesting optimal structures and atomic configurations and device designs.

There is a lush “garden” full of existing and imaginable atomic structures through which one can make small holes in many different ways (Figure 3c). This variety includes different pore sizes comparable to the ion sizes and different pore surface charges influencing transport, ion selectivity, *etc.* Transport is additionally dependent on the pH and the transport mechanism can be tuned *in situ* by changing the pH. As Geim and Grigorieva remarked in their Perspective on stacked 2D layers,<sup>68</sup> one can think of this “atomic engineering” as playing with “LEGO on atomic scale” and stacking 2D materials to make “van der Waals” pores<sup>70</sup> (Figure 3d). One can also use  $1 \times 1$  LEGO blocks, in analogy to individual atoms (Figure 3e) and start designing and building more complex, “size zero” atom-scale holes in three dimensions (Figure 3f). As with LEGO, pores and surfaces can be designed with step edges and nontrivial atomic structures. One such scenario of a “rugged atomic terrain” was imagined by Shankla *et al.*, who used molecular dynamics to model a “step defect” in multilayer graphene that can guide DNA motion.<sup>69</sup> Particularly important are those atoms at the edges of pores that can interact with the environment and govern the pore charge and other properties. With the advancement of analytical tools such as aberration-corrected microscopy and single-atom-resolution electron energy loss spectroscopy, one can directly probe and visualize the atomic structure of nanochannels and nanopores (*ex situ*, before and after ionic measurements) and investigate

directly the edge termination at the pore “walls” that can be relevant in describing observed transport properties arising from the pore structure and chemistry. Membrane materials can also be conducting, such as graphene, opening the door to a new class of nanopore devices in which electronic sensing and control are performed directly at the pore.<sup>25</sup> Similarly, illumination of 2D solid-state membranes such as 2D WS<sub>2</sub><sup>20</sup> (Figure 1b) may be exploited to control the ion transport, as recently exemplified by 2D MoS<sub>2</sub> membranes by Graf *et al.*<sup>71</sup>

**Final Remarks.** We expect this to be an exciting and dynamic decade for this growing interdisciplinary field, with experiments and theories dancing together, like the highly coupled ions and water molecules, as explained by Yao *et al.*<sup>3</sup> These two dance partners are steadily converging in their abilities to deal with the complexities involved. For experimental dancers, it is now increasingly possible to fabricate atomic-scale devices to know their atomic detail and to probe fluid transport through them. Reproducing key experimental results and developing careful interpretations is especially important in this field given the delicate nature of structures and measurements and the typically small device numbers measured and used to validate results. Theoretical dancers, on the other hand, with their numerical approaches and toolkits in hand, particularly atomistic molecular dynamics simulations, are now also better prepared to handle larger systems and the correspondingly large number of atoms involved in the real world to describe the measured phenomena accurately in existing environments. In practice, theory and experiment at the nanoscale tend to be different, but maybe one day, they can dance together as one. New ideas, concepts, and common terminology will probably be developed in this process. At these mesoscales, both single-ion and many-body descriptions are important. Physical, chemical, and biological approaches can benefit from and enjoy dancing together.

## AUTHOR INFORMATION

### Corresponding Author

**Marija Drndić** – Department of Physics and Astronomy, University of Pennsylvania, Philadelphia, Pennsylvania 19104, United States; [orcid.org/0000-0002-8104-2231](https://orcid.org/0000-0002-8104-2231); Email: [drndic@physics.upenn.edu](mailto:drndic@physics.upenn.edu)

### Authors

**Jothi Priyanka Thiruraman** – Department of Physics and Astronomy and Department of Electrical and Systems Engineering, University of Pennsylvania, Philadelphia, Pennsylvania 19104, United States; [orcid.org/0000-0001-5089-491X](https://orcid.org/0000-0001-5089-491X)

**Paul Masih Das** – Department of Physics and Astronomy, University of Pennsylvania, Philadelphia, Pennsylvania 19104, United States; [orcid.org/0000-0003-2644-2280](https://orcid.org/0000-0003-2644-2280)

Complete contact information is available at: <https://pubs.acs.org/10.1021/acsnano.0c01625>

### Notes

The authors declare no competing financial interest.

## ACKNOWLEDGMENTS

This work was supported in part by the National Institutes of Health under Grant No. R21HG010536 and by the National Science Foundation under Grant Nos. NSF EFRI-1542707, NSF EAGER 1838456, and NSF DMR 1905045 (“*In Situ*

TEM and *Ex Situ* Studies of Two-Dimensional Nanostructured Devices”). Fabrication work for Figure 3a,c was performed at the University of Pennsylvania’s Singh Center for Nanotechnology, an NNCI member supported by NSF Grant No. ECCS-1542153. We also acknowledge use of TEM facilities and instrumentation supported by the NSF through the University of Pennsylvania Materials Research Science and Engineering Center (DMR-1720530). We thank Dr. Douglas Yates of the University of Pennsylvania and Dr. Robert Keyse of Lehigh University for their assistance with STEM imaging. We thank Prof. Alex Noy for useful comments on their work featured in this Perspective,<sup>3</sup> and Prof. Adrien Nicolai for providing us the molecular dynamics model for Figure 3b. We also thank Milivoj Segan for his artistic representation of the MoS<sub>2</sub>–WS<sub>2</sub> bilayer pore by Masih Das *et al.* (Figure 3d)<sup>70</sup> and Dr. W. Parkin for making and imaging the two-dimensional MoS<sub>2</sub> pore in Figure 3a during his PhD work. The TEM image of the ion-irradiated, two-dimensional WS<sub>2</sub> membrane in Figure 3c was taken by Paul Masih Das and Jothi Priyanka Thiruraman during their PhD work.

## REFERENCES

- (1) Weinert, F.; *et al.* *Philos. Sci. Trav. Hist. Philos. Sci.* **2009**, 13–1, 99–133.
- (2) Danda, G.; Drndić, M. Two-Dimensional Nanopores and Nanoporous Membranes for Ion and Molecule Transport. *Curr. Opin. Biotechnol.* **2019**, 55, 124–133.
- (3) Yao, Y.-C.; Taqieddin, A.; Alibakhshi, M. A.; Wanunu, M.; Aluru, N. R.; Noy, A. Strong Electroosmotic Coupling Dominates Ion Conductance of 1.5 nm Diameter Carbon Nanotube Porins. *ACS Nano* **2019**, 13, 12851–12859.
- (4) Marcus, Y. Ionic Radii in Aqueous Solutions. *Chem. Rev.* **1988**, 88, 1475–1498.
- (5) Tongraar, A.; Liedl, K. R.; Rode, B. M. Born–Oppenheimer Ab Initio QM/MM Dynamics Simulations of Na<sup>+</sup> and K<sup>+</sup> in Water: From Structure Making to Structure Breaking Effects. *J. Phys. Chem. A* **1998**, 102, 10340–10347.
- (6) Feng, J.; Liu, K.; Graf, M.; Dumcenco, D.; Kis, A.; Di Ventra, M.; Radenovic, A. Observation of Ionic Coulomb Blockade in Nanopores. *Nat. Mater.* **2016**, 15, 850–855.
- (7) Esfandiari, A.; Radha, B.; Wang, F. C.; Yang, Q.; Hu, S.; Garaj, S.; Nair, R. R.; Geim, A. K.; Gopinadhan, K. Size Effect in Ion Transport through Angstrom-Scale Slits. *Science* **2017**, 358, 511–513.
- (8) Krems, M.; Di Ventra, M. Ionic Coulomb Blockade in Nanopores. *J. Phys.: Condens. Matter* **2013**, 25, No. 065101.
- (9) Russel, W. B. *Colloidal Dispersions*; Cambridge University Press: Cambridge, UK, 1989.
- (10) Tunuguntla, R. H.; Henley, R. Y.; Yao, Y.-C.; Pham, T. A.; Wanunu, M.; Noy, A. Enhanced Water Permeability and Tunable Ion Selectivity in Subnanometer Carbon Nanotube Porins. *Science* **2017**, 357, 792–796.
- (11) Branton, D.; Deamer, D. W.; Marziali, A.; Bayley, H.; Benner, S. A.; Butler, T.; Di Ventra, M.; Garaj, S.; Hibbs, A.; Huang, X.; Jovanovich, S. B.; Krstic, P. S.; Lindsay, S.; Ling, Z. S.; Mastrangelo, C. H.; Meller, A.; Oliver, J. S.; Pershin, Y. V.; Ramsey, J. M.; Riehn, R.; *et al.* The Potential and Challenges of Nanopore Sequencing. *Nat. Biotechnol.* **2008**, 26, 1146–1153.
- (12) Amiri, H.; Shepard, K. L.; Nuckolls, C.; Hernández Sánchez, R. Single-Walled Carbon Nanotubes: Mimics of Biological Ion Channels. *Nano Lett.* **2017**, 17, 1204–1211.
- (13) Secchi, E.; Nigues, A.; Jubin, L.; Siria, A.; Bocquet, L. Scaling Behavior for Ionic Transport and Its Fluctuations in Individual Carbon Nanotubes. *Phys. Rev. Lett.* **2016**, 116, 154501.
- (14) Manghi, M.; Palmeri, J.; Yazda, K.; Henn, F.; Jourdain, V. Role of Charge Regulation and Flow Slip on the Ionic Conductance of Nanopores: An Analytical Approach. *Phys. Rev. E: Stat. Phys., Plasmas, Fluids, Relat. Interdiscip. Top.* **2018**, 98, No. 012605.

- (15) Venta, K.; Shemer, G.; Puster, M.; Rodríguez-Manzo, J. A.; Balan, A.; Rosenstein, J. K.; Shepard, K.; Drndić, M. Differentiation of Short, Single-Stranded DNA Homopolymers in Solid-State Nanopores. *ACS Nano* **2013**, *7*, 4629–4636.
- (16) Rodríguez-Manzo, J. A.; Puster, M.; Nicolai, A.; Meunier, V.; Drndić, M. DNA Translocation in Nanometer Thick Silicon Nanopores. *ACS Nano* **2015**, *9*, 6555–6564.
- (17) Shekar, S.; Niedzwiecki, D. J.; Chien, C.-C.; Ong, P.; Fleischer, D. A.; Lin, J.; Rosenstein, J. K.; Drndić, M.; Shepard, K. L. Measurement of DNA Translocation Dynamics in a Solid-State Nanopore at 100 ns Temporal Resolution. *Nano Lett.* **2016**, *16*, 4483–4489.
- (18) Chien, C.-C.; Shekar, S.; Niedzwiecki, D. J.; Shepard, K. L.; Drndić, M. Single-Stranded DNA Translocation Recordings through Solid-State Nanopores on Glass Chips at 10 MHz Measurement Bandwidth. *ACS Nano* **2019**, *13*, 10545–10554.
- (19) Sawafta, F.; Carlsen, A.; Hall, A. Membrane Thickness Dependence of Nanopore Formation with a Focused Helium Ion Beam. *Sensors* **2014**, *14*, 8150–8161.
- (20) Danda, G.; Masih Das, P.; Chou, Y.-C.; Mlack, J. T.; Parkin, W. M.; Naylor, C. H.; Fujisawa, K.; Zhang, T.; Fulton, L. B.; Terrones, M.; Johnson, A. T. C.; Drndić, M. Monolayer WS<sub>2</sub> Nanopores for DNA Translocation with Light-Adjustable Sizes. *ACS Nano* **2017**, *11*, 1937–1945.
- (21) Danda, G.; Masih Das, P.; Drndić, M. Laser-Induced Fabrication of Nanoporous Monolayer WS<sub>2</sub> Membranes. *2D Mater.* **2018**, *5*, No. 035011.
- (22) Yamazaki, H.; Hu, R.; Zhao, Q.; Wanunu, M. Photothermally Assisted Thinning of Silicon Nitride Membranes for Ultrathin Asymmetric Nanopores. *ACS Nano* **2018**, *12*, 12472–12481.
- (23) Gilboa, T.; Zvuloni, E.; Zrehen, A.; Squires, A. H.; Meller, A. Automated, Ultra-Fast Laser-Drilling of Nanometer Scale Pores and Nanopore Arrays in Aqueous Solutions. *Adv. Funct. Mater.* **2019**, 1900642.
- (24) Waugh, M.; Briggs, K.; Gunn, D.; Gibeault, M.; King, S.; Ingram, Q.; Jimenez, A. M.; Berryman, S.; Lomovtsev, D.; Andrzejewski, L.; Tabard-Cossa, V. Solid-State Nanopore Fabrication by Automated Controlled Breakdown. *Nat. Protoc.* **2020**, *15*, 122–143.
- (25) Merchant, C. A.; Healy, K.; Wanunu, M.; Ray, V.; Peterman, N.; Bartel, J.; Fischbein, M. D.; Venta, K.; Luo, Z.; Johnson, A. T. C.; Drndić, M. DNA Translocation through Graphene Nanopores. *Nano Lett.* **2010**, *10*, 2915–2921.
- (26) Garaj, S.; Hubbard, W.; Reina, A.; Kong, J.; Branton, D.; Golovchenko, J. A. Graphene as a Subnanometre Trans-Electrode Membrane. *Nature* **2010**, *467*, 190–193.
- (27) Schneider, G. F.; Kowalczyk, S. W.; Calado, V. E.; Pandraud, G.; Zandbergen, H. W.; Vandersypen, L. M. K.; Dekker, C. DNA Translocation through Graphene Nanopores. *Nano Lett.* **2010**, *10*, 3163–3167.
- (28) Liu, K.; Feng, J.; Kis, A.; Radenovic, A. Atomically Thin Molybdenum Disulfide Nanopores with High Sensitivity for DNA Translocation. *ACS Nano* **2014**, *8*, 2504–2511.
- (29) Liu, S.; Lu, B.; Zhao, Q.; Li, J.; Gao, T.; Chen, Y.; Zhang, Y.; Liu, Z.; Fan, Z.; Yang, F.; You, L.; Yu, D. Boron Nitride Nanopores: Highly Sensitive DNA Single-Molecule Detectors. *Adv. Mater.* **2013**, *25*, 4549–4554.
- (30) Zhou, Z.; Hu, Y.; Wang, H.; Xu, Z.; Wang, W.; Bai, X.; Shan, X.; Lu, X. DNA Translocation through Hydrophilic Nanopore in Hexagonal Boron Nitride. *Sci. Rep.* **2013**, *3*, 3287.
- (31) Mojtavani, M.; VahidMohammadi, A.; Liang, W.; Beidaghi, M.; Wanunu, M. Single-Molecule Sensing Using Nanopores in Two-Dimensional Transition Metal Carbide (MXene) Membranes. *ACS Nano* **2019**, *13*, 3042–3052.
- (32) Wanunu, M.; Dadosh, T.; Ray, V.; Jin, J.; McReynolds, L.; Drndić, M. Rapid Electronic Detection of Probe-Specific MicroRNAs Using Thin Nanopore Sensors. *Nat. Nanotechnol.* **2010**, *5*, 807–814.
- (33) Larkin, J.; Henley, R.; Bell, D. C.; Cohen-Karni, T.; Rosenstein, J. K.; Wanunu, M. Slow DNA Transport through Nanopores in Hafnium Oxide Membranes. *ACS Nano* **2013**, *7*, 10121–10128.
- (34) Fischbein, M. D.; Drndić, M. Electron Beam Nanosculpting of Suspended Graphene Sheets. *Appl. Phys. Lett.* **2008**, *93*, 113107.
- (35) Feng, J.; Liu, K.; Bulushev, R. D.; Khlybov, S.; Dumcenco, D.; Kis, A.; Radenovic, A. Identification of Single Nucleotides in MoS<sub>2</sub> Nanopores. *Nat. Nanotechnol.* **2015**, *10*, 1070–1076.
- (36) Feng, J.; Graf, M.; Liu, K.; Ovchinnikov, D.; Dumcenco, D.; Heiranian, M.; Nandigana, V.; Aluru, N. R.; Kis, A.; Radenovic, A. Single-Layer MoS<sub>2</sub> Nanopores as Nanopower Generators. *Nature* **2016**, *536*, 197–200.
- (37) Garaj, S.; Liu, S.; Golovchenko, J. A.; Branton, D. Molecule-Hugging Graphene Nanopores. *Proc. Natl. Acad. Sci. U. S. A.* **2013**, *110*, 12192–12196.
- (38) Thiruraman, J. P.; Fujisawa, K.; Danda, G.; Das, P. M.; Zhang, T.; Bolotsky, A.; Perea-López, N.; Nicolai, A.; Senet, P.; Terrones, M.; Drndić, M. Angstrom-Size Defect Creation and Ionic Transport through Pores in Single-Layer MoS<sub>2</sub>. *Nano Lett.* **2018**, *18*, 1651–1659.
- (39) Smeets, R. M. M.; Keyser, U. F.; Dekker, N. H.; Dekker, C. Noise in Solid-State Nanopores. *Proc. Natl. Acad. Sci. U. S. A.* **2008**, *105*, 417–421.
- (40) Roux, B. Ion Channels and Ion Selectivity. *Essays Biochem.* **2017**, *61*, 201–209.
- (41) Gadsby, D. C. Ion Channels versus Ion Pumps: The Principal Difference, in Principle. *Nat. Rev. Mol. Cell Biol.* **2009**, *10*, 344–352.
- (42) Kowalczyk, S. W.; Grosberg, A. Y.; Rabin, Y.; Dekker, C. Modeling the Conductance and DNA Blockade of Solid-State Nanopores. *Nanotechnology* **2011**, *22*, 315101.
- (43) Venta, K. E.; Zanjan, M. B.; Ye, X.; Danda, G.; Murray, C. B.; Lukes, J. R.; Drndić, M. Gold Nanorod Translocations and Charge Measurement through Solid-State Nanopores. *Nano Lett.* **2014**, *14*, 5358–5364.
- (44) Siria, A.; Poncharal, P.; Bianco, A.-L.; Fulcrand, R.; Blase, X.; Purcell, S. T.; Bocquet, L. Giant Osmotic Energy Conversion Measured in a Single Transmembrane Boron Nitride Nanotube. *Nature* **2013**, *494*, 455–458.
- (45) Rollings, R. C.; Kuan, A. T.; Golovchenko, J. A. Ion Selectivity of Graphene Nanopores. *Nat. Commun.* **2016**, *7*, 11408.
- (46) Bocquet, L.; Charlaix, E. Nanofluidics, from Bulk to Interfaces. *Chem. Soc. Rev.* **2010**, *39*, 1073–1095.
- (47) Kim, D.-K.; Duan, C.; Chen, Y.-F.; Majumdar, A. Power Generation from Concentration Gradient by Reverse Electrodialysis in Ion-Selective Nanochannels. *Microfluid. Nanofluid.* **2010**, *9*, 1215–1224.
- (48) Plecis, A.; Schoch, R. B.; Renaud, P. Ionic Transport Phenomena in Nanofluidics: Experimental and Theoretical Study of the Exclusion-Enrichment Effect on a Chip. *Nano Lett.* **2005**, *5*, 1147–1155.
- (49) Caglar, M.; Silkina, I.; Brown, B. T.; Thornework, A. L.; Burton, O. J.; Babenko, V.; Gilbert, S. M.; Zettl, A.; Hofmann, S.; Keyser, U. F. Tunable Anion-Selective Transport through Monolayer Graphene and Hexagonal Boron Nitride. *ACS Nano* **2020**, DOI: 10.1021/acsnano.9b08168.
- (50) Liu, K.; Lihter, M.; Sarathy, A.; Caneva, S.; Qiu, H.; Deiana, D.; Tileli, V.; Alexander, D. T. L.; Hofmann, S.; Dumcenco, D.; Kis, A.; Leburton, J.-P.; Radenovic, A. Geometrical Effect in 2D Nanopores. *Nano Lett.* **2017**, *17* (7), 4223–4230.
- (51) Suk, M. E.; Aluru, N. R. Ion Transport in Sub-5-nm Graphene Nanopores. *J. Chem. Phys.* **2014**, *140*, No. 084707.
- (52) Wilson, J.; Aksimentiev, A. Water-Compression Gating of Nanopore Transport. *Phys. Rev. Lett.* **2018**, *120*, 268101.
- (53) Pérez, M. D. B.; Nicolai, A.; Delarue, P.; Meunier, V.; Drndić, M.; Senet, P. Improved Model of Ionic Transport in 2-D MoS<sub>2</sub> Membranes with Sub-5 nm Pores. *Appl. Phys. Lett.* **2019**, *114*, No. 023107.
- (54) Thiruraman, J. P.; Fujisawa, K.; Danda, G.; Das, P. M.; Zhang, T.; Bolotsky, A.; Perea-López, N.; Nicolai, A.; Senet, P.; Terrones, M.;

Drndić, M. Correction to Angstrom-Size Defect Creation and Ionic Transport through Pores in Single-Layer MoS<sub>2</sub>. *Nano Lett.* **2019**, *19*, 627–627.

(55) O'Hern, S. C.; Boutilier, M. S. H.; Idrobo, J.-C.; Song, Y.; Kong, J.; Laoui, T.; Atieh, M.; Karnik, R. Selective Ionic Transport through Tunable Subnanometer Pores in Single-Layer Graphene Membranes. *Nano Lett.* **2014**, *14*, 1234–1241.

(56) Jain, T.; Rasera, B. C.; Guerrero, R. J. S.; Boutilier, M. S. H.; O'Hern, S. C.; Idrobo, J.-C.; Karnik, R. Heterogeneous Sub-Continuum Ionic Transport in Statistically Isolated Graphene Nanopores. *Nat. Nanotechnol.* **2015**, *10*, 1053–1057.

(57) Hong, S.; Constans, C.; Surmani Martins, M. V.; Seow, Y. C.; Guevara Carrió, J. A.; Garaj, S. Scalable Graphene-Based Membranes for Ionic Sieving with Ultrahigh Charge Selectivity. *Nano Lett.* **2017**, *17*, 728–732.

(58) Hirunpinyopas, W.; Prestat, E.; Worrall, S. D.; Haigh, S. J.; Dryfe, R. A. W.; Bissett, M. A. Desalination and Nanofiltration through Functionalized Laminar MoS<sub>2</sub> Membranes. *ACS Nano* **2017**, *11*, 11082–11090.

(59) Parkin, W. M.; Balan, A.; Liang, L.; Das, P. M.; Lamparski, M.; Naylor, C. H.; Rodríguez-Manzo, J. A.; Johnson, A. T. C.; Meunier, V.; Drndić, M. Raman Shifts in Electron-Irradiated Monolayer MoS<sub>2</sub>. *ACS Nano* **2016**, *10*, 4134–4142.

(60) Thiruraman, J. P.; Masih Das, P.; Drndić, M. Irradiation of Transition Metal Dichalcogenides Using a Focused Ion Beam: Controlled Single-Atom Defect Creation. *Adv. Funct. Mater.* **2019**, *29*, 1904668.

(61) Yoon, K.; Rahnamoun, A.; Swett, J. L.; Iberi, V.; Cullen, D. A.; Vlasiouk, I. V.; Belianinov, A.; Jesse, S.; Sang, X.; Ovchinnikova, O. S.; Rondinone, A. J.; Unocic, R. R.; van Duin, A. C. T. Atomistic-Scale Simulations of Defect Formation in Graphene under Noble Gas Ion Irradiation. *ACS Nano* **2016**, *10*, 8376–8384.

(62) Sandner, A.; Preis, T.; Schell, C.; Giudici, P.; Watanabe, K.; Taniguchi, T.; Weiss, D.; Eroms, J. Ballistic Transport in Graphene Antidot Lattices. *Nano Lett.* **2015**, *15*, 8402–8406.

(63) Cupo, A.; Masih Das, P.; Chien, C.-C.; Danda, G.; Khariche, N.; Tristant, D.; Drndić, M.; Meunier, V. Periodic Arrays of Phosphorene Nanopores as Antidot Lattices with Tunable Properties. *ACS Nano* **2017**, *11*, 7494–7507.

(64) Masih Das, P.; Thiruraman, J. P.; Chou, Y.-C.; Danda, G.; Drndić, M. Centimeter-Scale Nanoporous 2D Membranes and Ion Transport: Porous MoS<sub>2</sub> Monolayers in a Few-Layer Matrix. *Nano Lett.* **2019**, *19*, 392–399.

(65) Reserbat-Plantey, A.; Kalita, D.; Han, Z.; Ferlazzo, L.; Autier-Laurent, S.; Komatsu, K.; Li, C.; Weil, R.; Ralko, A.; Marty, L.; Guéron, S.; Bendiab, N.; Bouchiat, H.; Bouchiat, V. Strain Superlattices and Macroscale Suspension of Graphene Induced by Corrugated Substrates. *Nano Lett.* **2014**, *14*, 5044–5051.

(66) Yu, H.; Gupta, N.; Hu, Z.; Wang, K.; Srijanto, B. R.; Xiao, K.; Geohagan, D. B.; Jakobson, B. I. Tilt Grain Boundary Topology Induced by Substrate Topography. *ACS Nano* **2017**, *11*, 8612–8618.

(67) Gao, Z.; Wang, S.; Berry, J.; Zhang, Q.; Gebhardt, J.; Parkin, W. M.; Avila, J.; Yi, H.; Chen, C.; Hurtado-Parra, S.; Drndić, M.; Rappe, A. M.; Srolovitz, D. J.; Kikkawa, J. M.; Luo, Z.; Asensio, M. C.; Wang, F.; Johnson, A. T. C. Large-Area Epitaxial Growth of Curvature-Stabilized ABC Trilayer Graphene. *Nat. Commun.* **2020**, *11*, 1–10.

(68) Geim, A. K.; Grigorieva, I. V. Van Der Waals Heterostructures. *Nature* **2013**, *499*, 419–425.

(69) Shankla, M.; Aksimentiev, A. Step-Defect Guided Delivery of DNA to a Graphene Nanopore. *Nat. Nanotechnol.* **2019**, *14*, 858–865.

(70) Masih Das, P.; Thiruraman, J. P.; Zhao, M.; Mandyam, S.; Johnson, A. T. C.; Drndić, M. Atomic-Scale Patterning in Two-Dimensional van Der Waals Superlattices. *Nanotechnology* **2019**, *31*, 105302.

(71) Graf, M.; Lihter, M.; Unuchek, D.; Sarathy, A.; Leburton, J.-P.; Kis, A.; Radenovic, A. Light-Enhanced Blue Energy Generation Using MoS<sub>2</sub> Nanopores. *Joule* **2019**, *3*, 1549–1564.